RSC Advances

PAPER

View Article Online
View Journal | View Issue

Cite this: *RSC Adv.*, 2021, **11**, 26368

Physico-chemical study of new supramolecular-architectured hybrid organic–inorganic sulfates incorporating diammoniumdiphenylsulfone cations†

Manel Bouguerra,[a] Adel Mahroug,[a] Agata Wróbel,[b] Damian Trzybiński,[b] Krzysztof Woźniak[b] and Mohamed Belhouchet*[a]

Two new hybrid organic–inorganic compounds, which incorporate 3,3′-diammoniumdiphenylsulfone or 4,4′-diammoniumdiphenylsulfone cations and sulfate anions, were synthesized and analyzed in detail. The crystal structures of both systems were established using single-crystal X-ray diffraction analysis. Crystallographic study revealed that the crystals of both investigated compounds were constructed of repeatedly occurring organic and inorganic layers and allowed the description of their structural features. Dense networks of N–H···O hydrogen bonds were found in both crystals. In addition, S–O···π contacts and weak C–H···O hydrogen bonds were identified in each analyzed crystal network. All intermolecular interactions were quantitatively described by Hirshfeld surface analysis. Furthermore, a ^{13}C NMR study was conducted for the grown crystals. The functional groups present in the titular compounds were also the subjects of IR and Raman spectral studies. Finally, TGA/DSC and UV-vis absorption measurements were performed and allowed the thermal and optical characterization of the titular materials.

Received 11th May 2021
Accepted 12th July 2021

DOI: 10.1039/d1ra03696c

rsc.li/rsc-advances

1. Introduction

The quest for new functional materials is an on-going project, which challenges scientists of different disciplines. In contempt of the wealth of information provided by a constantly increasing number of publications, it remains challenging to precisely predict, judiciously design and successfully synthesize any crystal even with the simplest chemical compounds and methods.[1–3] However, we have limited our research to a particular family of compounds that have organic–inorganic hydrogen bonds in their structure, more specifically, to the organic sulfates family, not only due to their simple crystallographic architectures but also for their magnificent properties. These compounds have been used for ferroelectricity,[4,5] ferroelasticity,[6] ionic liquids,[7] electrical properties,[8,9] sensing devices and in the field of nonlinear optics.[10,11] Indeed, hydrogen sulfate (HSO_4^-) and sulfate (SO_4^{2-}) anions are of prime importance in the chemical and metal industries, with essential applications in biology, catalysis, energy storing and optics.[12]

Amines present a high permanent dipole moment,[13,14] which can be reoriented in the crystal matrix, as demonstrated by previously reported inorganic salts of aliphatic amines, or, as in our case, organic sulfates and organic hydrogen sulfates. In the studied compounds, the orientation of anionic and cationic species facilitates the formation of expected N–H···O hydrogen bonds between nitrogen and sulfate oxygen atoms, which, together with strong hydrogen bonds of the O–H···O type, play a key role in molecular recognition. By dint of the highly polar nature of the sulfur oxygen bond, sulfoxides and sulfones are not only considered to be good hydrogen bond acceptors, but they can, moreover, promote the hydrogen donor feature by enhancing the acidity of the adjacent α-hydrogens.[15,16]

Further prompted by the anti-bacterial properties of diphenyl sulfones and the increased biological activity shown after their incorporation into some heterocyclic compounds, we chose to work with the simplest, oldest, cheapest and most active antibacterial sulfone: the 4,4′-diaminobiphenylsulfone molecule (DDS).[17,18] Not only does the nucleophilicity of the 4-NH_2–C_6H_4–SO_2 moiety enhance the intrinsic activity of this antibacterial compound[19] but there are also electron-releasing substituents that transmit electronic effects through the aromatic ring onto the sulfone group. This leads to an increase in the negative charge density allocated on the oxygen atoms of the sulfone group, which boosts dapsone activity.[20] In addition,

[a]*Physico-Chemistry of Solid State Laboratory, Department of Chemistry, Faculty of Sciences of Sfax, B. P. 1171, 3000, Sfax, Tunisia. E-mail: manel01bouguerra@gmail.com; belhouchet2002@gmail.com*

[b]*Biological and Chemical Research Centre, Faculty of Chemistry, University of Warsaw, Żwirki i Wigury 101, 02-089 Warsaw, Poland*

† Electronic supplementary information (ESI) available: Tables of crystallographic data, additional IR/Raman spectra, NMR, UV-vis and thermal patterns (PDF). CCDC 1889448 and 1889445. For ESI and crystallographic data in CIF or other electronic format see DOI: 10.1039/d1ra03696c

the strong hydrogen bonding ability of DDS promotes higher possibilities of interaction with polar solvent molecules and thus their potential incorporation during recrystallization.[21]

The literature points to some co-crystals of the organic molecule dapsone that did not only help to understand its structural properties but also its solubility and dissolution rate. Smith *et al.* have reported two multi-component crystalline systems that exhibit one proton-transfer salt structures.[22] In 2013, they reported the structure of a second salt of dapsone, with ρ-toluenesulfonic acid, in which all amine and aminium H atoms were involved in different hydrogen bonds.[23] Later in 2014, Jiang *et al.* reported six co-crystals of dapsone with sulfanilamide, flavone, luteolin, caffeine and 2(3H)-benzothiazolone.[24] Three polymeric co-crystals of dapsone and flavone with comprehensive characterizations were reported by He *et al.* in 2015.[25] Gaytan-Barrientos *et al.* (2015) described the crystal structures of two new hydrated sulfonate salts and evaluated their hydrogen bonding patterns.[26] Finally, with an approach closest to ours, in 2017 Benahsese *et al.* synthesized the hydrated tetra-nitrate salt of dapsone.[27] In addition, 3,3′-DDS was reported in the form of a complex with β-cyclodextrin, which resulted in the formation of a twisted intramolecular charge transfer state.[28] Alongside these, the interest in such materials was aroused within our own research group. A series of different organic–inorganic materials (namely 3-ammoniumphenylsulfone selenate, 3-aminophenylsulfone, 3-ammoniumphenylsulfone dihydrogenphosphate phosphoric acid and bis(3-ammoniumphenyl)sulfone dinitrate) were firstly obtained with Mahroug *et al.* in the period of 2011–2013.[29–31] By 2017, Kessentini *et al.* had also confirmed the formation of an organic–inorganic 3,3′-(DDS)$SnCl_6$ hybrid system stabilized by different types of hydrogen bonding that are distinguished by their interesting electric properties.[32]

Hence, we report here the synthesis, detailed crystallographic analysis, vibrational study, description of the thermal behavior and the optical properties of two new hybrid organic–inorganic salts, namely 4,4′-diammoniumdiphenylsulfone sulfate (**4,4′-DDS-S**) and 3,3′-diammoniumdiphenylsulfone sulfate (**3,3′-DDS-S**). The outcomes serve to build a detailed background to better understand in which practical applications the new compounds could preferentially be applied.

2. Experimental

2.1. Synthesis

2.1.1. Synthesis of 4,4′-diammoniumdiphenylsulfone sulfate. An aqueous solution of sulfuric acid (2 mmol, 99.99%, purchased from Merck) was poured dropwise into 1 mmol of 4,4′-diaminodiphenylsulfone (97%, purchased from Merck) dissolved in ethanol (99.99%, purchased from Aldrich). All of the products were used without any further purification. The resulting solution was stirred continually for around one hour and then left to evaporate at room temperature for few days until the appearance of colorless crystals of **4,4′-DDS-S**.

2.1.2. Synthesis of 3,3′-diammoniumdiphenylsulfone sulfate. An aqueous solution of sulfuric acid (2 mmol, 99.99%, purchased from Merck) was added to 2 mmol of 3,3′-diaminodiphenyl sulfone (98%, purchased from Merck) dissolved in ethanol. The resulting solution was agitated steadily for around one hour and then left to evaporate at room temperature for few days until the appearance of colorless crystals of **3,3′-DDS-S**.

2.2. Experimental

2.2.1. Single-crystal X-ray diffraction analysis. Good-quality single-crystals of **4,4′-DDS-S** and **3,3′-DDS-S** were selected for X-ray diffraction experiments at $T = 100(2)$ K. The crystals were mounted with paratone-N oil using the MiTeGen micromount. Diffraction data were collected on an Agilent Technologies SuperNova Dual Source diffractometer with Cu Kα radiation ($\lambda = 1.54184$ Å) using CrysAlis RED software.[33] The multi-scan empirical absorption correction using spherical harmonics, implemented in the SCALE3 ABSPACK scaling algorithm, was applied.[33] The structural determination procedure was carried out using the SHELX package.[34] The structures were solved with direct methods and then successive least-squares refinement was carried out based on the full-matrix least-squares method on F^2 using the SHELXL program.[35] All of the H atoms linked to the N atoms were located on the Fourier difference electron density map and refined using $U_{iso}(H) = 1.2U_{eq}(N)$. The N–H bond lengths were restrained to 0.87 Å. The remaining H atoms were positioned geometrically with C–H equal to 0.93 Å and constrained to ride on their parent atoms with $U_{iso}(H) = 1.2U_{eq}(C)$. Molecular interactions in the crystals of both compounds were identified using the PLATON program.[36] The figures for this publication were prepared using Olex2, Mercury and ORTEP-3 programs.[37–39] Simulated PXRD patterns of both compounds were generated along the refinement process (Fig. S1 and S2†).

2.2.2. Spectroscopic measurements. The infra-red spectra were recorded, using a JASCOFT-IR-420 spectrometer, on each of the two crystal samples over the range of wave numbers from 4000 to 400 cm^{-1} with a resolution of about 4 cm^{-1}.

Furthermore, the Raman spectra were recorded with a Senterra dispersive μ-Raman spectrometer (Bruker) in the frequency range of 1800–100 cm^{-1}. The radiation wavelength of $\lambda = 785$ mm was chosen from the excitation and the spectral resolution was kept between 3–5 cm^{-1}.

2.2.3. NMR spectroscopy. Both NMR spectra were obtained on a Bruker DSX-300 spectrometer operating at 75.49 MHz, with a classical 4 mm probe head allowing spinning rates up to 10 kHz. ^{13}C chemical shifts are given relative to tetramethylsilane.

2.2.4. Thermal analysis. A thermoanalyzer, SETARAM type TG-ATD92, was used for the TGA measurements. The manipulations were carried out in air with a constant heating rate of 10 °C min^{-1} on fine samples, arranged in a platinum boat.

The differential scanning calorimetry (DSC) measurements were carried out using a SETARAM differential scanning calorimeter of the STA 449C type, also used in an air atmosphere.

3. Results and discussion

3.1. Description of the crystal structure

The identities of both investigated compounds were confirmed by the single-crystal X-ray diffraction analysis. The crystal and structure refinement details are presented in Table S1 (ESI).†

The full list of bond lengths, valence and torsion angle values is provided in the ESI (Tables S2–S7†).

4,4′-DDS-S and **3,3′-DDS-S** crystallize in the monoclinic $P2_1$ and $P2_1/c$ space groups, respectively. In both cases, the asymmetric unit of the crystal lattice comprises two crystallographically independent ionic pairs of the compound (Fig. 1).

The results of the crystallographic analysis clearly showed that all amine groups attached to the phenyl moieties within cations of both analyzed crystals are protonated. Therefore, all cationic species present in the crystals of **4,4′-DDS-S** and **3,3′-DDS-S** have a 2+ charge. Different positions of the $-NH_3$ substituents in the phenyl rings of the diphenyl sulfone moieties result in noticeable changes in the geometry of the above denoted cations. This difference is well illustrated by the angle values between the mean-planes of their adjacent phenyl rings. In **4,4′-DDS-S**, the mean planes of the above rings are inclined to themselves by 120.73(12) and 122.24(13)° for cation A and B, respectively. Concurrently, in the second compound (**3,3′-DDS-S**), the diphenyl sulfone core is much more bent. This feature is reflected by significantly lower values of the mentioned angle (91.18(14)° for cation A and 98.64(14)°) for the cation A and B).

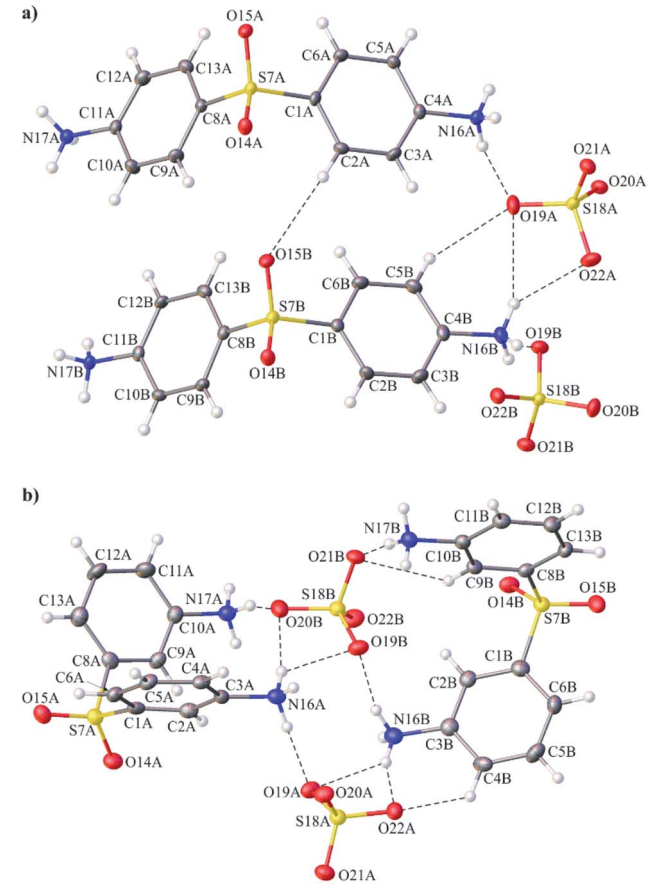

Fig. 1 Asymmetric unit of the crystal lattice of 4,4′-DDS-S (a) and 3,3′-DDS-S (b) with crystallographic atom numbering. Displacement ellipsoids are drawn at the 50% probability level. The H atoms are shown as small spheres of an arbitrary radius. The intermolecular N–H···O and C–H···O hydrogen bonds are represented by dashed lines.

Whilst analyzing the overall shape of the mentioned moiety, attention should be drawn to the value of its C–S–C valence angle. Thus, the values of the given parameter in **4,4′-DDS-S** are 107.84(17) for cation A and 107.61(17)° for B; whereas for **3,3′-DDS-S** slightly lower values of the above angle are found (100.28(18) and 103.22(19)° for cations A and B, respectively. By comparing the values of the above-mentioned parameters for both investigated compounds with those from other multi-component systems containing the 4,4′-diamine diphenyl and the 3,3′-diamine diphenyl sulfone moieties[40] (Table 1), it can be seen that the cationic moieties within these compounds are characterized by the considerable variability of their internal geometry. A possible explanation for this feature might be the different surroundings of these moieties in their crystals and the participation of their structural fragments in different schemes of intermolecular interactions.

In Table 1, *A* is the distance between the geometric centers of gravity of the adjacent phenyl rings within the diphenyl sulfone core and *B* is the angle between the mean planes of the adjacent phenyl ring within the diphenyl sulfone core.

As for the anionic species compensating the charge of the cations in the crystals of **4,4′-DDS-S** and **3,3′-DDS-S**, all of them have slightly distorted tetrahedral geometry (Fig. 2 (ref. 41)). The S–O bond lengths and the O–S–O valence angle values are within the ranges of 1.462(3)–1.493(3) Å and 107.60(16)–111.34(15)° for **4,4′-DDS-S** and 1.451(3)–1.501(3) Å and 103.30(18)–112.32(18)° for **3,3′-DDS-S**.

The packing of ions in the crystals of the examined salts exhibits interesting structural features. A close look at Fig. 3 reveals that both systems exhibit a layered supramolecular architecture.

In the case of **4,4′-DDS-S**, the layers are built exclusively from cations and anions alternately spread along the (101) direction (Fig. 3a). The ions labelled as A and B within each cationic or anionic layer are organized according to an ABAB scheme (Fig. 3a). The landscape of the intermolecular interactions in the crystal network is dominated by hydrogen bonds. Adjacent cations interact *via* two different weak C–H···O hydrogen bonds (d(D···A) = 3.343(5) and 3.388(5) Å; <(D–H···A) = 152 and 161°; Table S8† and Fig. 4a). In the case of the above mentioned cationic layers, seven different S–O···π contacts between the cations have been additionally identified (d(X···A) = 3.515(3) – 3.861(3) Å; <(D–X···A) = 94.86(12)°; Table S9†). These cations further interact with the neighbouring anions by means of a dense network of N–H···O hydrogen bonds (d(D···A) = 2.683(5) – 3.362(5) Å; <(D–H···A) = 124(3) and 169(4)°; Table S8† and Fig. 4a). Detailed analysis performed using the PLATON program allowed the identification of sixteen different interactions of this type. The resultant complex framework of ions is additionally stabilized by a network of four different C–H···O hydrogen bonds, which involve neighbouring cations and anions (d(D···A) = 3.175(5)–3.501(5) Å; <(D–H···A) = 123–169°; Table S8† and Fig. 4a). Interestingly, when looking at the packing of ions within the crystal of **4,4′-DDS-S** along the *a* direction, it can be seen that the mutual arrangement of the diamine diphenyl sulfone cations resembles a 'herring-bone' (Fig. 4a).

Table 1 Selected geometrical parameters describing the shape of the diphenyl sulfone core within **4,4′-DDS-S**, **3,3′-DDS-S** and their close structural relatives

Compound	*A* [Å]	*B* [°]	C–S–C [°]
4,4′-DDS-S	5.218(2)/5.229(2)	120.73(12)/122.24(13)	107.84(17)/107.16(17)
3,3′-DDS-S	4.595(2)/4.841(2)	91.18(14)/98.64(14)	100.28(18)/103.22(19)
4,4′-Sulfonyldianilinium dinitrate[40]	4.890(2)	100.86(7)	103.44(9)
3,3′-Sulfonyldianilinium bis(dihydrogen phosphate) phosphoric acid solvate[29]	5.052(2)	108.92(6)	105.02(7)

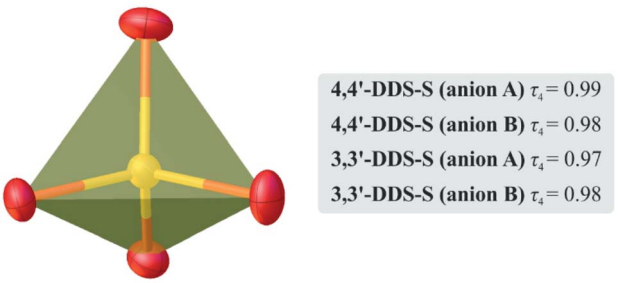

Fig. 2 Graphical representation of one of the tetrahedral SO^{2-} anions in the crystals of the investigated materials. The values of the τ_4 parameter[41] calculated for the individual cations A and B present in the structure are in the gray box.

The cations and ions in the crystal of the second crystalline multi-component system, **3,3′-DDS-S**, are also arranged in separate layers (Fig. 3b), however detailed comparison of its packing with that observed for **4,4′-DDS-S** allows us to notice significant differences between them.

In the case of **3,3′-DDS-S**, the infinite layers composed of both types of ions extend along the (011) plane. Most importantly, the cationic species are uniquely organized in bilayers constituted exclusively by cations labelled as A or B. Adjacent A cations inside these bilayers are linked together by two different C–H···O hydrogen bonds (d(D···A) = 3.088(5) and 3.420(6) Å; <(D–H···A) = 133 and 150°; Table S10† and Fig. 4b) and one S–O···π contact (d(X···A) = 3.195(4) Å; <(D–X···A) = 136.51(16)°; Table S11†). In turn, the cations labelled as B within their respective bilayers interact with each other by only one weak C–H···O hydrogen bond (d(D···A) = 3.178(5) Å; <(D–H···A) = 133°; Table S10† and Fig. 4b) and one S–O···π contact (d(X···A) = 3.143(3) Å; <(D–X···A) = 141.31(14)°; Table S11†). Between the above-defined and parallel to each other cationic bilayers of A and B, we distinguish a monolayer of anions, where sulfate ions are arranged in an AABB manner (Fig. 3b). Adjacent cations and anions in this formed 3D framework interact with themselves *via* sixteen different N–H···O hydrogen bonds (d(D···A) = 2.723(4)–3.165(5) Å; <(D–H···A) = 121(4) – 177(3)°; Table S10† and Fig. 4b). Finally, the whole crystal network is stabilized by a framework of three different C–H···O hydrogen bonds (d(D···A) = 3.178(5) – 3.357(5) Å; <(D–H···A) = 124–154°; Table S10† and Fig. 4b) between species with opposite charges.

The structures of both analyzed hybrid materials have comparable values for the packing indices. Thus, **4,4′-DDS-S** and **3,3′-DDS-S** occupy 70.94 and 70.44% of the volume of their unit cells, respectively.

3.2. Hirshfeld surface analysis

Hirshfeld surface analysis enables the quantitative description of intermolecular interactions occurring within the crystal lattice. Therefore, it allows us to develop more in-depth conclusions pertaining to the supramolecular architecture of

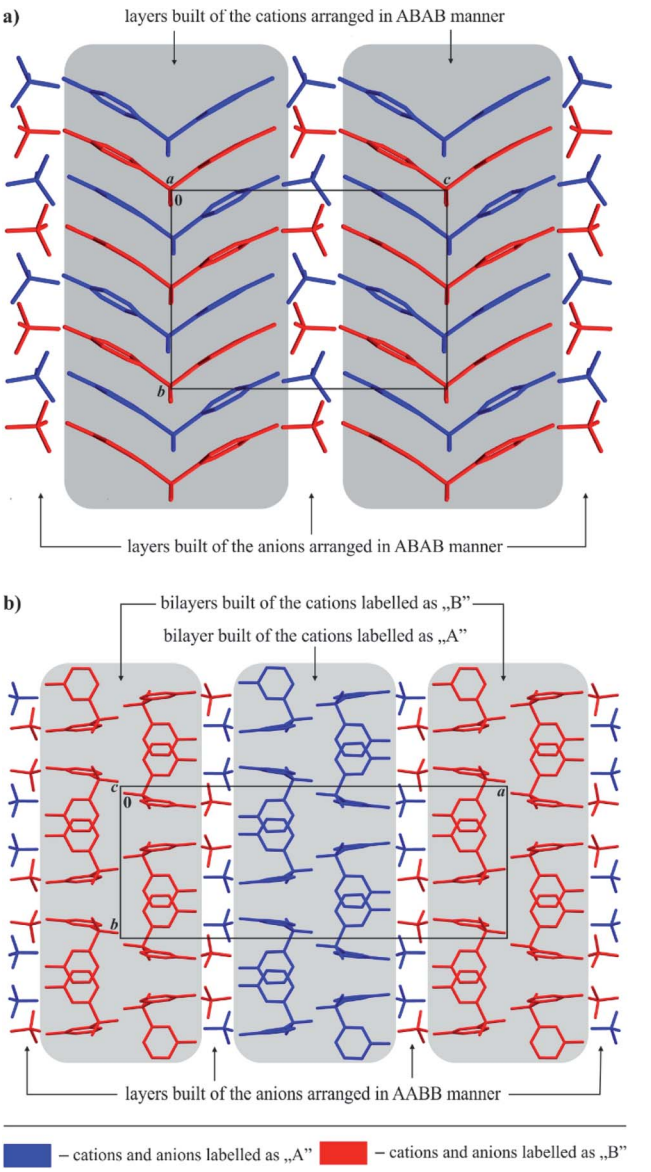

Fig. 3 General view of the layered supramolecular architecture of ions in the crystals of **4,4′-DDS-S** (a) and **3,3′-DDS-S** (b).

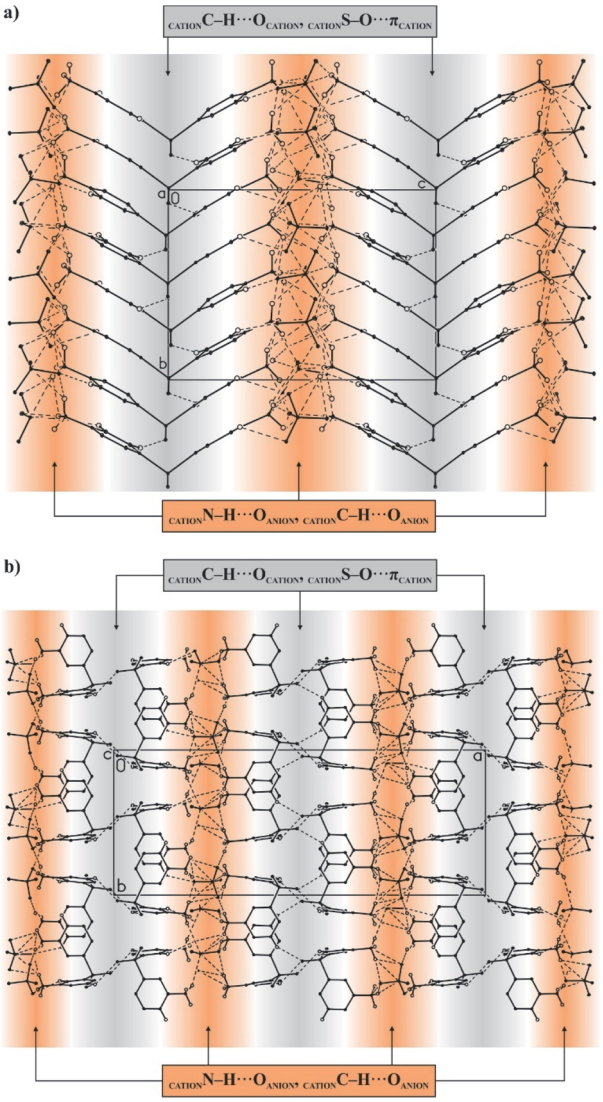

Fig. 4 Supramolecular architecture of crystals of 4,4′-DDS-S (a) and 3,3′-DDS-S (b). The areas where individual types of interactions occur have been highlighted in orange and grey. The hydrogen bonds are represented by dashed lines. The H atoms not participating in the intermolecular interactions have been omitted for clarity.

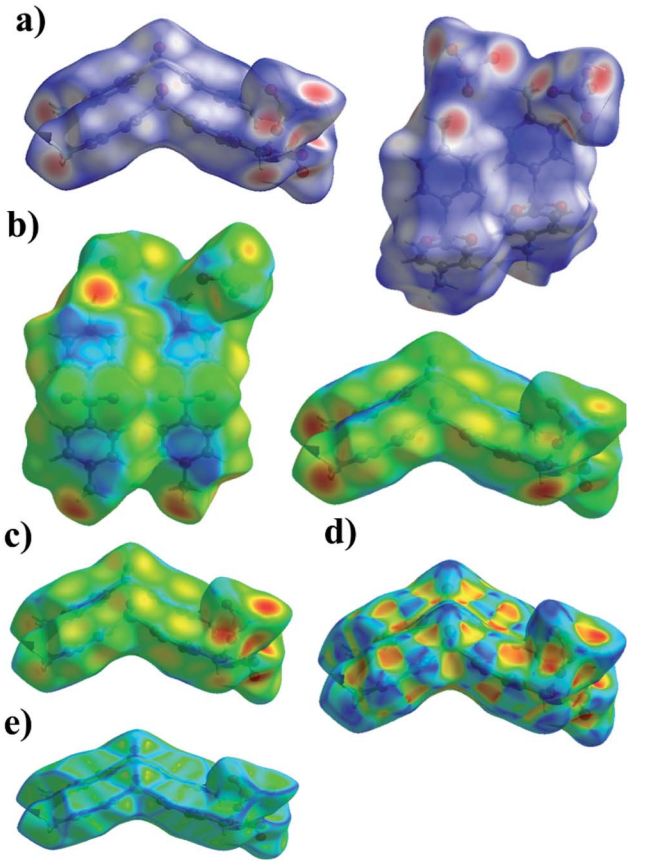

Fig. 5 The 3D representation of the Hirshfeld surface of 4,4′-DDS-S, mapped with d_{norm} (a), d_i (b), d_e (c), shape index (d) and curvedness (e).

the investigated systems. In case of the titular compounds, it was effectively deployed to visualize and formulate the similarities and differences noted in the molecular environments of their ions. For this purpose, the normalized contact distance (d_{norm}) feature of the computed Hirshfeld surface, based on the internal d_i and external d_e distance, was employed. The corresponding 3D maps of the Hirshfeld surfaces, where d_{norm} is visualized, are shown in Fig. 5 and 6. It should be noted that regions with an intense red color are located over the oxygen and the nitrogen atoms pertaining to the organic cations. These hot spots are attributed to the hydrogen bonds in which these atoms are participating.

The shape index, a measure of the total Hirshfeld map curvature, was mapped for both salts in the range of −1 Å (concave) to 1 Å (convex) (as displayed in Fig. 5d and 6d). In this feature of the Hirshfeld surface, the interactions between molecules are interpreted *via* the concaveness or convexness of the surface. Thus, domains presenting a concave curve shape are associated with acceptor regions (denoted in red), while those with a convex curve shape are attributed to donor regions of the molecule (denoted in blue). The curvedness of the surface in the presented maps ranged from −4 to 4 Å. In the cases of both analyzed systems, the prevailing green flat areas are separated by convex blue edges characterized by high values of curvedness (Fig. 5e and 6e).

The analysis of the 2D fingerprint plots of the Hirshfeld surfaces of both salts (Fig. 7 and 8) confirms that their crystal networks are dominated by intermolecular hydrogen bonds. The occurrence of this type of interaction is reflected in the 52.5 and 46.2% contribution of the O···H interatomic contacts to the total Hirshfeld surface of **4,4′-DDS-S** and **3,3′-DDS-S**, respectively. The presence of the N–H···O hydrogen bonds within the crystal structures also manifests itself by the presence of two sharp, symmetric spikes on both plots. Other interatomic contacts were also identified, however with relatively smaller shares. Among them, it is worth paying attention to the H···H, C···O, C···H and C···C interatomic contacts. These types of interactions make up 22.5, 10.6, 9.2 and 3.9% of the total contribution to the HS of **4,4′-DDS-S** and 24.7, 5.5, 16.3 and 3.9% for **3,3′-DDS-S**, respectively. Notably, the presence of the

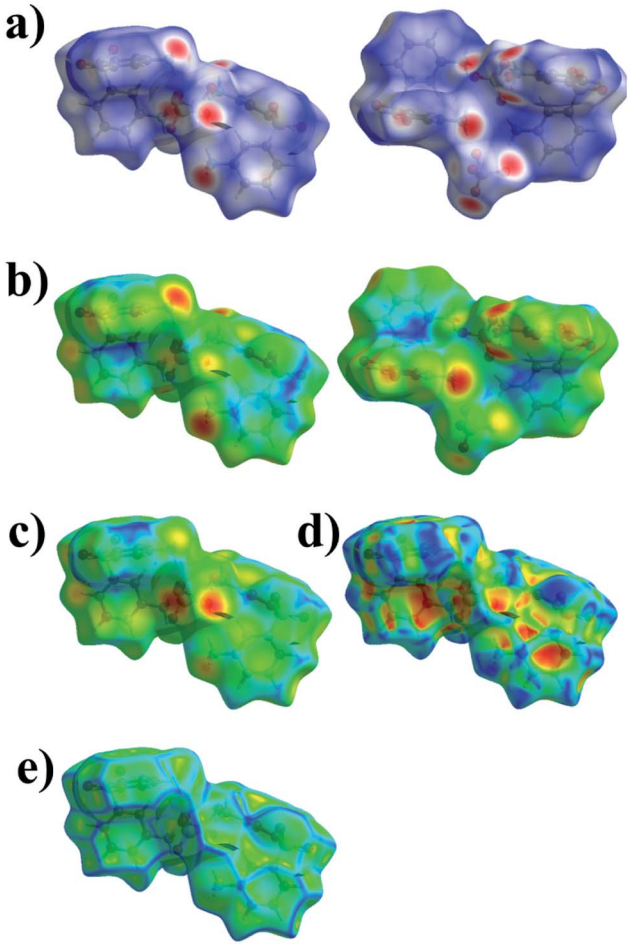

Fig. 6 The 3D representation of the Hirshfeld surface of 3,3′-DDS-S, mapped with d_{norm} (a), d_i (b), d_e (c), shape index (d) and curvedness (e).

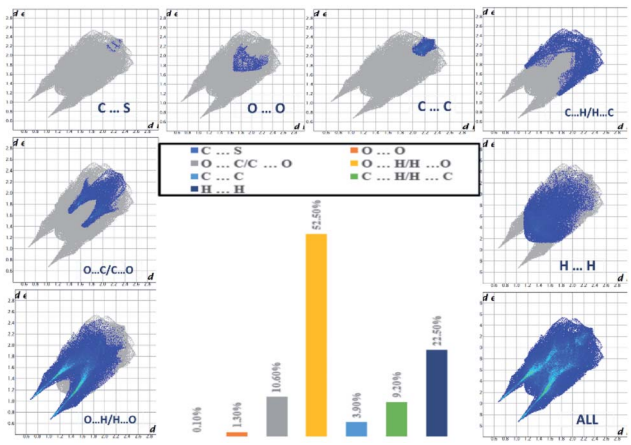

Fig. 7 The 2D fingerprint plots of the calculated Hirshfeld surface with the percentage contribution of various interatomic contacts occurring in the crystal of 4,4′-DDS-S.

C···O and C···C interatomic contacts proved the occurrence of the S–O···π and π–π contacts between adjacent cations within the investigated crystals. Finally, the O···O and C···S contacts

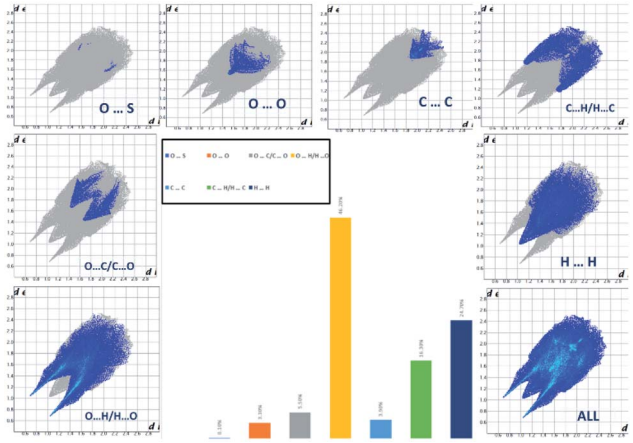

Fig. 8 The 2D fingerprint plots of the calculated Hirshfeld surface with the percentage contribution of various interatomic contacts occurring in the crystal of 3,3′-DDS-S.

were identified in the cases of both salts, but their contribution to the total Hirshfeld surfaces is minor. Their shares are 1.3% and 0.1% for **4,4′-DDS-S** and 3.3% and 1.3% for **3,3′-DDS**, respectively.

3.3. Vibrational study

Vibrational study is a handy tool to correlate structural and physical properties and its major purpose is to determine the vibrational variations of every group of atoms when they are irradiated by an electromagnetic wave of adequate frequency.[42]

The assignment of the different observed bands was carried out by homologous reference to analogical studies on corresponding organic molecules[10,43–45] and sulfuric acid.[46]

3.3.1. Vibrational study of 4,4′-DDS-S. The IR spectrum of this organic–inorganic material is illustrated in Fig. S3 (ESI†) and its Raman spectrum in Fig. S4 (ESI).† Table S12 (ESI†) brings together the attribution of the different vibration modes to the corresponding different organic and inorganic groups.

The symmetrical deformation vibration ν_2 of the sulfate group is represented by an average intensity line at 455 cm^{-1} in the IR spectrum and at the same value in the Raman spectrum. The peak with the strongest intensity, located at 1072 cm^{-1} in the IR spectrum and observed in the Raman spectrum at around 1072 cm^{-1}, is assigned to the asymmetric elongation mode ν_3 of the SO_4 moiety. All of the peaks appearing in the 616–550 cm^{-1} infrared frequency range are attributed to the asymmetric deformation mode ν_4 of the sulfate group. This vibration mode appears in the Raman spectrum in the form of a low-intensity line at 613 cm^{-1}. The symmetrical elongation vibration ν_1 of the sulfate group appears as two intense peaks in the IR and Raman spectra at around 963 cm^{-1}. These different attributions are comparable with the values observed for similar compounds[8,47–51].

The vibration modes $\delta_s(NH_3)$ and $\delta_{as}(NH_3)$ appear in the IR spectrum between 1602 and 1579 cm^{-1}, while in the Raman spectrum they show up as a single peak at around 1603 cm^{-1}. Peaks occurring between 2604 and 1936 cm^{-1} in the IR

spectrum are attributed to the vibrations ν(N–H···O). The two peaks that appear at 3470 and 3070 cm^{-1} in the same spectrum are from the elongation mode ν(N–H) of the NH_3 group. These modes are most likely caused by the different hydrogen bridges ensuring the cohesion of the two organic and inorganic entities. Furthermore, the different vibration modes of the SO_2 group are observed at 1297, 1134 and 490 cm^{-1} in the IR spectrum and at 1220, 1153 and 493 cm^{-1} in the Raman spectrum. The δ(C–C–C)$_{Ar}$ vibration modes emerge between 455 and 963 cm^{-1} in the IR spectrum and in the Raman spectrum between 974 and 455 cm^{-1}. The elongation vibration of the C=C double bond is manifested in the infrared spectrum as a band with an average intensity around 1482 cm^{-1} and a less intense band around 1497 cm^{-1}. In the Raman spectrum, this vibration mode is observed at around 1501 cm^{-1}. The ν(C–S) and ν(C–N) frequencies are mainly visible between 632 and 1057 cm^{-1} in the IR spectrum and between 633 and 1193 cm^{-1} in the Raman spectrum. The weak vibrations, observed in the [188, 288 cm^{-1}] area of the Raman spectrum, are related to the translational motions of the molecular lattice.

3.3.2. Vibrational study of 3,3′-DDS-S. The IR spectrum of **3,3′-DDS-S** is illustrated in Fig. S5 (ESI).† Compared to that of **4,4′-DDS-S**, the symmetrical deformation vibration ν_2 of the sulfate group in this case is represented by an intense peak at 458 cm^{-1}. The peak with a strong intensity located at 1151 cm^{-1} is assigned to the asymmetric elongation mode ν_3 of SO_4. The peak appearing at 618 cm^{-1} is attributed to the asymmetric deformation mode ν_4 of the sulfate group. The symmetrical elongation vibration ν_1 of the sulfate group appears as two intense peaks at 1077 and 965 cm^{-1}.

The vibration modes $\delta_s(NH_3)$ and $\delta_{as}(NH_3)$ appear between 1597 and 1564 cm^{-1}. Peaks occurring between 2597 and 1934 cm^{-1} are attributed to the vibrations ν(N–H···O). The molecules present more atomic inter-vibrations, which is why there is a rise in these values. The peaks that appear between 3563 and 3056 cm^{-1} are related to the elongation modes of the $(NH_3)^+$ group. Moreover, the different vibration modes of the SO_2 group are observed at 1219, 1151 and 485 cm^{-1}. The δ(C–C–C)$_{Ar}$ vibration modes emerge at around 430 cm^{-1}. The elongation vibration of the C=C double bond is manifested as a band appearing between 1501 and 1498 cm^{-1}. The ν(C–S) and ν(C–N) frequencies are mainly visible at 1318, 1206, 1040 and 697 cm^{-1}.

These different attributions, gathered in Table S12 (ESI†) do agree with those of the first presented compound as well as with similar systems, taking into consideration the different vibrational effects and distances.[52–55]

3.4. ^{13}C nuclear magnetic resonance

Nuclear magnetic resonance (NMR) is one of the most powerful spectroscopic techniques used to determine the structure of both organic and inorganic species. It relies on the magnetism of the nucleus.[56]

3.4.1. NMR study of 4,4′-DDS-S. The MAS ^{13}C NMR spectrum, presented in Fig. S6 (ESI†), reveals the presence of eight resolved peaks. The performed structural analysis has shown that, within the organic cation of **4,4′-DDS-S**, four types of carbon atoms with the same chemical environment are present. Thus, an attempt to attribute such peaks was made based on similar compounds and on the chemical shift of the organic molecule alone.[57,58]

The first two peaks at 124.3 ppm and at 126.32 ppm were assigned to the nuclei of carbon atoms of the first type (C5A, C3A, C10A and C12A, and C5B, C3B, C10B and C12B, respectively) The second signals centered at 131.21 ppm and at 132.55 ppm were assigned to aromatic carbons of the second type (C6A, C2A, C9A and C13A, and C6B, C2B, C9B and C13B). The signals of the third type of carbons (C1A and C8A, and C1B and C8B) were observed at 137.14, 140.35 and 141.58 ppm. The fourth peak at 152.33 ppm was assigned to fourth type of carbons (C4A and C11A, and C4B and C11B). The positions of the MAS ^{13}C NMR peaks, as well as their allocations, are presented in Table S13 (ESI†).

3.4.2. NMR study of 3,3′-DDS-S. Unlike the first compound, the MAS ^{13}C NMR spectrum of **3,3′-DDS-S**, presented in Fig. S7 (ESI†), showed seven resolved peaks, each assigned to a different carbon type. The first peak, situated at 124.50 ppm, was assigned to C2A and C9A, and C2B and C9B. The peaks at 125.93 and 129.24 ppm were attributed to C4A and C11A, and C4B and C11B. The fourth peak, centered at 144.30 ppm, was assigned to C6A and C13A, and C6B and C13B. C5A and C12A, and C5B and C12B were observed at 151.30 ppm. The signal at 156.61 ppm was attributed to C1A and C8A, and C1B and C8B. And finally, the peak at 161.92 was assigned to C3A and C10A, and C3B and C10B.

3.5. Thermal study

The thermal behaviors of 13 mg of each of the synthesized compounds were studied by TGA coupled to DSC in the temperature range from 25–600 °C under an air atmosphere with a heating rate of 10 °C min^{-1}.

The DSC curve recorded for **4,4′-DDS-S** is presented in Fig. 9. As expected, transformations arise at a temperature of 230 °C, where the organic entity engages in a combustion process. As a result, CO_2, CO, SO_2 and H_2O are released in the gas form, as proven by partial thermal specific tracking. Relative figures can be found in the ESI (Fig. S8–S11†).

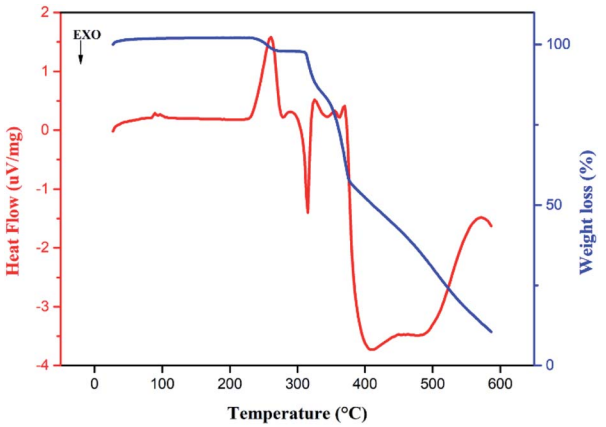

Fig. 9 The TGA–DSC analysis curves recorded for 4,4′-DDS-S.

The endothermic peak at 260 °C in the DSC curve, coupled with a minor loss of mass, characterizes the departure of water molecules, supported by data from Fig. S11.† It is followed by more significant weight loss taking place between 280 °C and 600 °C, which is, consequently, assigned to the degradation of the material into the previously mentioned gas forms. This attribution is moreover supported by previous studies on similar compounds.[59–61]

As for **3,3′-DDS-S**, the thermogravimetric analysis curve (Fig. 10) shows two mass losses. The first small loss, which takes place between 200 °C and 280 °C, corresponds to the departure of H_2O moieties, as depicted in Fig. S12.† Whereas the second important loss, starting from 300 °C, represents the degradation of the compound into the same released gases as the first compound (Fig. S13–S15†). Other studies have shown similar thermal behavior.[62–65]

It is to be noted that the release of SO_2 gas underlines the role of S–O···π contacts in increasing the solidity of the crystal packing. Due to **3,3′-DDS-S** having fewer counted S–O···π contacts (two S–O···π contacts), it emits SO_2 gas in a very tight range of temperature (between 300–380 °C). This is unlike the **4,4′-DDS-S** compound that exhibits a wider temperature range of the release of this gas, between 300 °C and 460 °C approximately, owing to the seven S–O···π contacts.

On the other hand, despite the same counted C–H···O interactions, **3,3′-DDS-S** demonstrates a tighter range of temperature for the elimination of CO and CO_2 gases that starts almost 100 °C later than that for the **4,4′-DDS-S** sample. This highlights that C–H···O interactions are much stronger in the molecular arrangement of **3,3′-DDS-S**.

3.6. UV-visible spectroscopy study

In order to investigate the possibility of using our compounds in NLO applications, we used UV-vis spectroscopy.

The UV-visible spectrum recorded for **4,4′-DDS-S**, shown in Fig. S16 (ESI†), exhibits three different bands in the UV range. The first one is observed at $\lambda = 214.83$ nm and the second is observed at 257.06 nm. The last band appears at about 290.00 nm. With reference to similar compounds,[66–69] these three peaks can be assigned to the $\pi \rightarrow \pi^*$ transitions of the organic cation. The absence of absorption in the visible region, as well as the crystallization in the non-centrosymmetric monoclinic $P2_1$ space group, could mean that it is possible to obtain a microscopic NLO response with non-zero values.[70,71] As a matter of fact, further theoretical calculations (DFT) could allow us to obtain the values of polarizability and hyperpolarizability, which would enable us to preview the NLO response of this non-centrosymmetric material.[72]

The ultraviolet spectroscopic study carried out on **3,3′-DDS-S** in the wavelength range from 200 to 700 nm is illustrated in Fig. S17 (ESI†). The peak detected at 215.04 nm can be attributed to the $\pi \rightarrow \pi^*$ transition. In the visible region, no optical transmission has been detected, which suggests the ability of our compound to be a good crystal for second harmonic generation (SHG), once some enhancements (such as the Corona poling technique) are applied, as previously done in comparable centrosymmetric compounds.[73,74]

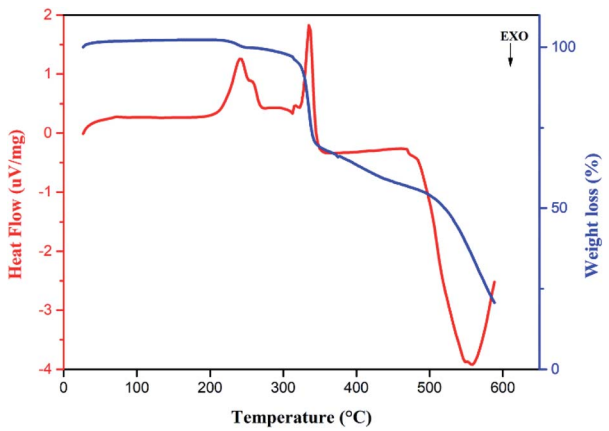

Fig. 10 The TGA–DSC analysis curves recorded for 3,3′-DDS-S.

4. Conclusions

In this work, the synthesis and physicochemical characterization of new organic–inorganic hybrid materials of two diaminodiphenyl sulfone derivatives (**3,3′-DDS-S** and **4,4′-DDS-S**) was reported. The undertaken crystallographic investigations allowed us to confirm the identity of both systems and to understand their structural features in the solid state. Therefore, it was possible to demonstrate the occurrence of cationic monolayers in the crystal of **4,4′-DDS-S** or bilayers in the crystal of **3,3′-DDS-S** intertwined with anionic layers. This supramolecular architecture was found to prompt the formation of desirable N–H···O and C–H···O hydrogen bond networks between adjacent ions in both crystal networks. The cationic layers in both investigated systems were additionally stabilized by the presence of S–O···π contacts between neighboring cations within these supramolecular entities. The landscapes of the intermolecular interactions occurring in **4,4′-DDS-S** and **3'3'-DDS-S** were also corroborated and quantitatively demonstrated by HS analysis. Additionally, ^{13};C NMR, IR and Raman spectral studies were also carried out for substance characterization. The temperature stability of the titular compounds was tested *via* TGA–DSC analysis and, finally, the optical properties of the compounds were examined by UV-vis absorption, where a number of $\pi \rightarrow \pi^*$ transitions were designated. The NLO potential activity of the studied compounds could be derived from further calculations. To sum up, we believe that the research results presented within this paper enrich the current state of knowledge concerning hybrid multi-component crystalline systems based on diaminodiphenyl sulfones and we hope that they will draw the attention of other researchers to this interesting group of compounds.

Author contributions

The manuscript was written with the contributions of all authors. All authors have approved the final version of the manuscript.

Conflicts of interest

There are no conflicts to declare.

Acknowledgements

This study was carried out at the Biological and Chemical Research Centre, University of Warsaw, established within the project co-financed by the European Union from the European Regional Development Fund under the Operational Programme Innovative Economy, 2007–2013. The X-ray diffraction data collection was done as part of the "core facility for crystallographic and biophysical research to support the development of medicinal products" project. The "Core facility for crystallographic and biophysical research to support the development of medicinal products" project is carried out within the TEAM-TECH Core Facility programme of the Foundation for Polish Science, co-financed by the European Union under the European Regional Development Fund.

References

1 G. Shubha, M. Tejaswini and K. Lakshmi, Advanced Material For Newer Applications, *Mater. Today: Proc.*, 2018, **5**(1), 2541–2546.

2 Z. Liu, M. Meyers, Z. Zhang and R. Ritchie, Functional Gradients And Heterogeneities In Biological Materials: Design Principles, Functions, And Bioinspired Applications, *Prog. Mater. Sci.*, 2017, **88**, 467–498.

3 Y. Li, X. Zou, W. Qiu, A. You, Z. Zhang, A. Feng and X. Chen, Design And Synthesis Of Porous 3D Mofs Hybrid Functional Materials Encapsulating Macrocyclic Metal Complexes, *Inorg. Chem. Commun.*, 2018, **94**, 114–118.

4 M. Mostafa, T. El Dean and A. Tammam, Characterization, Phase Change And Conductivity Crossover Of New Luminescent Ferroelectric Mn(II) Organic–Inorganic Hybrid, *Mater. Chem. Phys.*, 2016, **180**, 373–382.

5 T. Apih, V. Žagar and J. Seliger, NMR And NQR Study Of Above-Room-Temperature Molecular Ferroelectrics Diisopropylammonium Chloride And Diisopropylammonium Perchlorate, *J. Phys. Chem. C*, 2016, **120**(11), 6180–6189.

6 M. Owczarek, R. Jakubas, I. Majerz and J. Baran, Experimental (IR) And Theoretical (LDA) Studies Of The Structure And Vibrational-Reorientational Dynamics Of Ferroelastic 1-Aminopyridinium Iodide, *Chem. Phys.*, 2012, **405**, 167–174.

7 A. Kobryn, S. Gusarov and K. Shankar, Multiscale Modeling Of Active Layer Of Hybrid Organic–Inorganic Solar Cells For Photovoltaic Applications By Means Of Density Functional Theory And Integral Equation Theory Of Molecular Liquids, *J. Mol. Liq.*, 2019, **289**, 110997.

8 J. Cihelka, D. Havlíček, R. Gyepes, I. Němec and Z. Koleva, *S*-(−)-1-Phenyl Ethyl Ammonium(1+) Sulphate And *S*-(−)-1-Phenyl Ethyl Ammonium(1+) Hydrogen Phosphate 2.5 Hydrate, Preparation And Characterization Of Crystallographic, Optical And Dielectric Properties, *J. Mol. Struct.*, 2010, **980**(1–3), 31–38.

9 W. Bednarski, A. Ostrowski and S. Waplak, Influence Of Mn^{2+} Doping Level On Conductivity Of $(NH_4)_3H(SO_4)_2$ Superprotonic Conductor, *Solid State Ionics*, 2008, **179**(35–36), 1974–1979.

10 A. Barhoumi, T. Mhiri, T. Dammak, J. Suñol and M. Belhouchet, Structural Characterization, Vibrational Study, NLO And DFT Calculations Of A Novel Organic Sulfate Monohydrate Templated With (*S*)-(−)-2,6-Diammonium-4,5,6,7-Tetrahydrobenzothiazole, *J. Mol. Struct.*, 2017, **1128**, 544–551.

11 I. Guezguez, A. Ayadi, K. Ordon, K. Iliopoulos, D. Branzea, A. Migalska-Zalas, M. Makowska-Janusik, A. El-Ghayoury and B. Sahraoui, Zinc Induced A Dramatic Enhancement Of The Nonlinear Optical Properties Of An Azo-Based Iminopyridine Ligand, *J. Phys. Chem. C*, 2014, **118**(14), 7545–7553.

12 Y. Zhang, C. Chen, G. Xu and W. Xin, Synthesis, Characterization And Temperature-Triggered Phase Transition Of Organic–Inorganic Hybrid Compound: $(C_6H_{18}N_2)(HSO_4)_2$, *J. Mol. Struct.*, 2019, **1176**, 1–6.

13 M. Farasat, S. Shojaei, M. Golzan and K. Farhadi, Theoretical Study Of The Potential Energy Surface And Electric Dipole Moment Of Aniline, *J. Mol. Struct.*, 2016, **1108**, 341–346.

14 C. Maridevarmath and G. Malimath, Computational And Experimental Studies On Dielectric Relaxation And Dipole Moment Of Some Anilines And Phenol, *J. Mol. Liq.*, 2017, **241**, 845–851.

15 o. Almarsson and M. Zaworotko, Crystal Engineering Of The Composition Of Pharmaceutical Phases. Do Pharmaceutical Co-Crystals Represent A New Path To Improved Medicines?, *Chem. Commun.*, 2004, (17), 1889–1896.

16 K. S. Eccles, C. J. Elcoate, S. P. Stokes, A. R. Maguire and S. E. Lawrence, Sulfoxides: Potent Co-Crystal Formers, *Cryst. Growth Des.*, 2010, **10**(10), 4243–4245.

17 E. F. Elslager, Z. B. Gavrilis, A. A. Phillips and D. F. Worth, Repository Drugs. IV. 4′,4‴-Sulfonylbisacetanilide (Acedapsone,DADDS) and Related Sulfanilylanilides with Prolonged Antimalarial and Antileprotic Action, *J. Med. Chem.*, 1969, **12**(3), 357–363.

18 S. Barbuceanu, G. Almajan, I. Saramet, C. Draghici, R. Socoteanu and F. Barbuceanu, New S-Alkylated 1,2,4-Triazoles Incorporating Diphenyl Sulfone Moieties with Potential Antibacterial Activity, *J. Serb. Chem. Soc.*, 2009, **74**(10), 1041–1049.

19 P. G. De Benedetti, D. Iarossi, C. Menziani, V. Caiolfa, C. Frassineti and C. Cennamo, Quantitative Structure-Activity Analysis in Dihydropteroate Synthase Inhibition of Sulfones. Comparison with Sulfanilamides, *J. Med. Chem.*, 1987, **30**(3), 459–464.

20 P. G. De Benedetti, U. Folli, D. Iarossi and C. Frassineti, Experimental and Theoretical Study of Electronic Substituent Effects in 4-Aminoaryl (4-Substituted Aryl) Sulphones, *J. Chem. Soc., Perkin Trans. 2*, 1985, (10), 1527.

21 H. Lemmer, N. Stieger, W. Liebenberg and M. R. Caira, Solvatomorphism of the Antibacterial Dapsone: X-Ray

Structures and Thermal Desolvation Kinetics, *Cryst. Growth Des.*, 2012, **12**(3), 1683–1692.

22 G. Smith and U. D. Wermuth, 4-(4-Aminophenylsulfonyl) Aniline–1,3,5-Trinitrobenzene (1/2), *Acta Crystallogr., Sect. E: Struct. Rep. Online*, 2012, **68**(2), o494.

23 G. Smith and U. D. Wermuth, 4-(4-Aminophenylsulfonyl) Anilinium Toluene-4-Sulfonate, *Acta Crystallogr., Sect. E: Struct. Rep. Online*, 2013, **70**(1), 0–9.

24 L. Jiang, Y. Huang, Q. Zhang, H. He, Y. Xu and X. Mei, Preparation and Solid-State Characterization of Dapsone Drug–Drug Co-Crystals, *Cryst. Growth Des.*, 2014, **14**(9), 4562–4573.

25 H. He, L. Jiang, Q. Zhang, Y. Huang, J.-R. Wang and X. Mei, Polymorphism Observed in Dapsone–Flavone Cocrystals That Present Pronounced Differences in Solubility and Stability, *CrystEngComm*, 2015, **17**(34), 6566–6574.

26 N. S. Gaytán-Barrientos, D. Morales-Morales, D. Herrera-Ruiz, R. Reyes-Martínez and J. Rivera-Islas, Sulfonate Salts of the Therapeutic Agent Dapsone: 4-[(4-Aminophenyl) Sulfonyl]Anilinium Benzenesulfonate Monohydrate and 4-[(4-Aminophenyl)Sulfonyl]Anilinium Methanesulfonate Monohydrate, *Acta Crystallogr., Sect. C: Struct. Chem.*, 2016, **72**(4), 280–284.

27 A. H. Benahsene, L. Bendjeddou and H. Merazig, Crystal Structure of Bis[Bis(4-Azaniumylphenyl)Sulfone] Tetranitrate Monohydrate, *Acta Crystallogr., Sect. E: Crystallogr. Commun.*, 2017, **73**(11), 1721–1725.

28 M. V. Enoch, R. Rajamohan and M. Swaminathan, Fluorimetric and Prototropic Studies on the Inclusion Complexation of 3,3′-Diaminodiphenylsulphone with β-Cyclodextrin and Its Unusual Behavior, *Spectrochim. Acta, Part A*, 2010, **77**(2), 473–477.

29 A. Mahroug, M. Belhouchet and T. Mhiri, Synthesis and Crystal Structure of 3-Ammoniumphenyl Sulfone Selenate, 3-Aminophenyl Sulfone $[C_{12}H_{14}N_2O_2S]SeO_4\cdots[C_{12}H_{12}N_2O_2S]$, *Crystallogr. Rep.*, 2013, **58**(4), 613–616.

30 A. Mahroug, M. Belhouchet, A. Hémon-Ribaud and T. Mhiri, Synthesis, Crystal Structure, and Characterization of a New Adduct 3-Ammoniumphenyl Sulfone Dihydrogenphosphate Phosphoric Acid $[C_{12}H_{14}N_2SO_2](H_2PO_4)_2H_3PO_4$, *Phosphorus, Sulfur Silicon Relat. Elem.*, 2011, **186**(12), 2332–2340.

31 A. Mahroug, M. Belhouchet and T. Mhiri, Synthesis and Crystal Structure of Bis(3-Ammoniumphenyl) Sulfone Dinitrate $[C_{12}H_{14}N_2O_2S](NO_3)_2$, *Crystallogr. Rep.*, 2013, **58**(4), 608–612.

32 A. Kessentini, T. Dammak and M. Belhouchet, Synthesis, Molecular Structure, Vibrational Spectroscopy, Optical Investigation and DFT Study of a Novel Hybrid Material: 3,3′-Diammoniumdiphenylsulfone Hexachloridostannate Monohydrate, *J. Mol. Struct.*, 2017, **1149**, 818–827.

33 Oxford Diffraction, *CrysAlis CCD and CrysAlis RED*, Oxford Diffraction Ltd, Yarnton, 2008.

34 G. M. Sheldrick. *SHELXS-97 Program for Crystal Solution*, University of Gottingen, Germany, 1997.

35 G. M. Sheldrick. *SHELXL-97 Program for Crystal Structure Refinement*, University of Gottingen, Germany, 1997.

36 A. L. Spek, Structure Validation in Chemical Crystallography, *Acta Crystallogr., Sect. D: Biol. Crystallogr.*, 2009, **65**(2), 148–155.

37 O. V. Dolomanov, L. J. Bourhis, R. J. Gildea, J. A. Howard and H. Puschmann, OLEX2: A Complete Structure Solution, Refinement and Analysis Program, *J. Appl. Crystallogr.*, 2009, **42**(2), 339–341.

38 C. F. Macrae, I. J. Bruno, J. A. Chisholm, P. R. Edgington, P. McCabe, E. Pidcock, L. Rodriguez-Monge, R. Taylor, J. van de Streek and P. A. Wood, Mercury CSD 2.0– New Features for the Visualization and Investigation of Crystal Structures, *J. Appl. Crystallogr.*, 2008, **41**(2), 466–470.

39 L. J. Farrugia, WinGXandORTEP for Windows: An Update, *J. Appl. Crystallogr.*, 2012, **45**(4), 849–854.

40 A. H. Benahsene, R. Henchiri, N. Ennaceur, M. Carcelli, H. Merazig and L. Bendjeddou, Two Nitrates of Dapsone: New Candidates for Non-Linear Optical Materials, *J. Mol. Struct.*, 2019, **1178**, 375–383.

41 L. Yang, D. R. Powell and R. P. Houser, Structural Variation in Copper(I) Complexes with Pyridylmethylamide Ligands: Structural Analysis with a New Four-Coordinate Geometry Index, τ4, *Dalton Trans.*, 2007, (9), 955–964.

42 H. G. Brittain. *Polymorph. Pharm. Solids*, 2nd edn, 2016, pp. 347–380.

43 C. Ben Hassen, T. Dammak, N. Chniba-Boudjada, T. Mhiri and M. Boujelbene, Chemical Synthesis, Crystal Structure, Vibrational Spectroscopy, Non-Linear Optical Properties and DFT Calculation of Bis (2,6-Diaminopyridinium) Sulfate Monohydrate, *J. Mol. Struct.*, 2017, **1127**, 43–52.

44 T. B. Issa and L. Benhamada, Crystal Structure, Thermal Behavior and Vibrational Spectra of 4,4′Diamoniumdiphenylmethan Sulfate Hydrate, *Open J. Inorg. Chem.*, 2017, **07**(02), 61–73.

45 R. D'Cunha, V. B. Kartha and S. Gurnani, Raman and I. r. Studies of the Antileprotic Drug Dapsone, *Spectrochim. Acta, Part A*, 1983, **39**(4), 331–336.

46 R. M. Bell and M. A. Jeppesen, The Raman Spectrum of Sulphuric Acid, *J. Chem. Phys.*, 1935, **3**(5), 245–247.

47 K. Hoxha and T. J. Prior, Retention of Crystallinity in Bis(Guaninium) Sulfate Hydrate upon Partial and Full Dehydration, *Solid State Sci.*, 2013, **23**, 102–108.

48 R. E. Khoma, V. O. Gelmboldt, V. N. Baumer, O. V. Shishkin and L. V. Koroeva, Synthesis and Structure of Aminoguanidinium Sulfite Monohydrate, *Russ. J. Inorg. Chem.*, 2013, **58**(7), 843–847.

49 B. R. Srinivasan, S. S. Khandolkar, R. N. Jyai, K. Ravikumar, B. Sridhar and S. Natarajan, Structural and Spectral Characterization of a New Non-Centrosymmetric Organic Thiosulfate, *Spectrochim. Acta, Part A*, 2013, **102**, 235–241.

50 I. Matulková, J. Cihelka, M. Pojarová, K. Fejfarová, M. Dušek, P. Vaněk, J. Kroupa, R. Krupková, J. Fábry and I. Němec, A New Series of 3,5-Diamino-1,2,4-Triazolium(1+) Inorganic Salts and Their Potential in Crystal Engineering of Novel NLO Materials, *CrystEngComm*, 2012, **14**(14), 4625.

51 T. J. Bednarchuk, V. Kinzhybalo, E. Markiewicz, B. Hilczer and A. Pietraszko, Structure, Dielectric and Electric

Properties of Diisobutylammonium Hydrogen Sulfate Crystal, *J. Solid State Chem.*, 2018, **258**, 753–761.

52 S. Guidara, H. Feki and Y. Abid, Structural, Vibrational, NLO, MEP, NBO Analysis and DFT Calculation of Bis 2,5-Dimethylanilinium Sulfate, *J. Mol. Struct.*, 2015, **1080**, 176–187.

53 R. E. Khoma, V. O. Gel'mbol'dt, V. N. Baumer, A. N. Puzan and A. A. Ennan, Methylammonium Sulfate: Synthesis and Structure, *Russ. J. Inorg. Chem.*, 2015, **60**(10), 1199–1203.

54 T. Sahbani, W. Smirani, S. S. Al-Deyab and M. Rzaigui, Synthesis and Characterization of a New Organic Sulphate, $[2,3\text{-}(CH_3)_2C_6H_3NH_3]HSO_4\cdot H_2O$, *Mater. Res. Bull.*, 2012, **47**(6), 1455–1458.

55 A. Chtioui, L. BenHamada and A. Jouini, Crystal Structure, Thermal Analysis and IR Spectrometric Investigation of Bis(*o*-Anisidinium) Sulfate $(C_7H_{10}NO)_2SO_4$, *Mater. Res. Bull.*, 2009, **44**(3), 560–565.

56 D. G. Gusev, NMR in Organometallic Chemistry. By Paul S. Pregosin, *Angew. Chem., Int. Ed.*, 2012, **51**(52), 12930–12931.

57 J. Oueslati, A. Oueslati, C. Ben Nasr and F. Lefebvre, Synthesis and Crystal Structure of a New Adduct of Dihydrogenphosphate Phosphoric Acid Monohydrate with 8-Aminoquinolinium, *Solid State Sci.*, 2006, **8**(9), 1067–1073.

58 S. Soukrata, M. Belhouchet, K. Adil and T. Mhiri, Synthesis, Structural Characterization and Thermal Behavior of New Organic–Inorganic Sulfate, *J. Cluster Sci.*, 2015, **26**(4), 1413–1424.

59 C. E. Wyman and N. D. Hinman, Ethanol, *Appl. Biochem. Biotechnol.*, 1990, **24–25**(1), 735–753.

60 E. I. Sal'nikova, Y. G. Denisenko, A. S. Aleksandrovsky, I. E. Kolesnikov, E. Lähderanta, P. O. Andreev, N. O. Azarapin, O. V. Andreev, S. A. Basova and A. V. Matigorov, Synthesis and Optical Properties RE2O2S:Ln (RE = La, Y; Ln = Ce, Eu, Dy, Er), *J. Solid State Chem.*, 2019, **279**, 120964.

61 Y. G. Denisenko, V. V. Atuchin, M. S. Molokeev, A. S. Aleksandrovsky, A. S. Krylov, A. S. Oreshonkov, S. S. Volkova and O. V. Andreev, Structure, Thermal Stability, and Spectroscopic Properties of Triclinic Double Sulfate $AgEu(SO_4)_2$ with Isolated SO_4 Groups, *Inorg. Chem.*, 2018, **57**(21), 13279–13288.

62 S. Saïd, S. Elleuch, K. Ślepokura, T. Lis and H. Naïli, Crystal Structure, Thermal Analysis and IR Spectrometric Investigation of the Tris(2,6-Diaminopyridinium) Hydrogen Sulfate Sulfate Monohydrate, *J. Mol. Struct.*, 2016, **1114**, 189–196.

63 T. Sahbani, A. C. Dhieb, W. S. Smirani and M. Rzaigui, Synthesis, Structural Characterization, Hirshfeld Surface Analysis, Spectroscopic and Ferroelectric Properties Studies of 4-Methylbenzylammonium Sulfate, *Phase Transitions*, 2017, **90**(6), 557–568.

64 C. Ben Hassen, M. Boujelbene, S. Marweni, M. Bahri and T. Mhiri, Synthesis, Crystal Structure, Thermal Analysis and Vibrational Spectroscopy Accomplished with DFT Calculation of New Hybrid Compound $[2\text{-}CH_3C_6H_4NH_3]HSO_4.H_2O$, *J. Mol. Struct.*, 2015, **1098**, 229–239.

65 I. Matulková, J. Cihelka, K. Fejfarová, M. Dušek, M. Pojarová, P. Vaněk, J. Kroupa, M. Šála, R. Krupková and I. Němec, Semi-Organic Salts of Aniline with Inorganic Acids: Prospective Materials for the Second Harmonic Generation, *CrystEngComm*, 2011, **13**(12), 4131–4138.

66 Y. Kessentini, A. B. Ahmed, S. S. Al-Juaid, T. Mhiri and Z. Elaoud, Synthesis and Non Linear Optical Properties of New Inorganic–Organic Hybrid Material: 4-Benzylpiperidinium Sulfate Monohydrate, *Opt. Mater.*, 2016, **53**, 101–108.

67 B. Helina, Growth and Characterization of the Semiorganic Nonlinear Optical Crystal: Diglycine Ammonium Sulfate, *Optik*, 2016, **127**(3), 1401–1404.

68 A. Abbas, H. Gökce and S. Bahçeli, Spectroscopic (Vibrational, NMR and UV-Vis.) and Quantum Chemical Investigations on 4-Hexyloxy-3-Methoxybenzaldehyde, *Spectrochim. Acta, Part A*, 2016, **152**, 596–607.

69 C. Ben M'leh, S. A. Brandán, N. Issaoui, T. Roisnel and H. Marouani, Synthesis, Molecular Structure, Vibrational and Theoretical Studies of a New Non-Centrosymmetric Organic Sulphate with Promising NLO Properties, *J. Mol. Struct.*, 2018, **1171**, 771–785.

70 A. Roshan S, C. Joseph and M. A. Ittyachen, Growth and Characterization of a New Metal–Organic Crystal: Potassium Thiourea Bromide, *Mater. Lett.*, 2001, **49**(5), 299–302.

71 V. Venkataramanan, S. Maheswaran, J. N. Sherwood and H. L. Bhat, Crystal Growth and Physical Characterization of the Semiorganic Bis(Thiourea) Cadmium Chloride, *J. Cryst. Growth*, 1997, **179**(3–4), 605–610.

72 N. Elleuch, W. Amamou, A. Ben Ahmed, Y. Abid and H. Feki, Vibrational Spectroscopic Study, Charge Transfer Interaction and Nonlinear Optical Properties of L-Asparaginium Picrate: A Density Functional Theoretical Approach, *Spectrochim. Acta, Part A*, 2014, **128**, 781–789.

73 V. Nalla, R. Medishetty, Y. Wang, Z. Bai, H. Sun, J. Wei and J. J. Vittal, Second Harmonic Generation from the "Centrosymmetric" Crystals, *IUCrJ*, 2015, **2**, 317–321.

74 G. Tellier, D. Averty, E. Blart, C. Boisrobert, H. Gundel, S. Le Tacon, C. Monnereau, F. Odobel and R. Seveno, Polymer Poling Characterization Using Second Harmonic Generation (SHG), *Organic Optoelectronics and Photonics II*, 2006, 6192.